

Characteristics of single key transients on the flute

Leon Bilton (z5204123)

Supervised by André Almeida and Joe Wolfe

Science Vacation Research Scholarship Report (UGVC1056)

UNSW Acoustics

Abstract

Single-key legato note transients are investigated for the flute. The static regime response at transitional key openings is recorded for $F4 \leftrightarrow F\#4$ and $D4 \leftrightarrow F\#4$ transients. A pump and recorder mouthpiece provide reproducible playing. Results show nonlinear frequency variation, with most of the transition occurring for a near-closed tone hole. The $D4 \leftrightarrow F\#4$ response requires a larger aperture change to saturate at the new note. Inside-outside transfer functions are also measured for the transitional geometries, and Helmholtz resonance theory is used to determine the inertance and effective acoustical length of the tone hole. The inertance increases from $151.52 \pm 39.13 \text{ Pa m}^{-3} \text{ s}^{-2}$ to $402.9 \text{ Pa m}^{-3} \text{ s}^{-2}$ during key closure, while the ratio of effective length to physical aperture height approaches 6:1 for a near-closed key. The static regime observations are compared to real time transient recordings. The observations confirm that key speed affects the results, introducing distinctions between closing and opening responses.

I Introduction

The steady state and excitation mechanics for the flute, and woodwind instruments in general, are well studied and can be explained in terms of aerodynamic and acoustical principles [1]. This understanding has allowed for more detailed research into harmonic generation and instrument timbre. Analysis and classification of instrument timbre is of importance to digital audio technologies, as well as instrument manufacturers. Instruments of the woodwind family are particularly challenging in this regard, since they all produce similar note features in overlapping frequency ranges, making them difficult to distinguish. Recent work in this lab has been focused on detailed inspection of initial and final transients [2] [3], which are of proven importance in timbre classification [4]. However, the significance of transitional effects between notes remains relatively undetermined. Promising initial results were demonstrated by Campbell and Heller (1978), who referred to the transitional region as the *legato transient*. Various experiments have since reinforced these findings [5] [6].

This project is focused on flute transients from an already established note to a nearby note, achieved by opening or closing a single key without alteration of the input flow. The frequency of the produced note varies with key opening, however the relationship is not trivial.

This is briefly discussed in a previous project by Almeida, Chow, *et al.* concerning the effects of fingering coordination on the transient sound [7]. Measurement of frequency changes during the transition is difficult, since average mechanical transition times for single key movements are on the order of tens of milliseconds. Therefore, it is helpful to record the playing frequency for a range of static key openings. Furthermore, the relationship between playing frequency and key opening involves the acoustical effect of the inertia of air beneath the key. In other words, the mechanical limits of the key, i.e. spring-controlled compression of the key foot and player-controlled compression of the key pad, may not directly correspond to acoustically open or closed states. For a comparison of transition times, finding the geometries that correspond to these effectively open/closed states is required. These will be hereafter referred to as the *effectively open/closed geometries*.

II Playing frequency for static geometries

Due to the short timescales of typical note transitions, analysis of the frequency variation using the Discrete Fourier Transform method involves a large compromise in frequency resolution. For this reason, it was useful to analyse the playing frequency for intermediate key positions. These static regime responses could give an indication of the effectively open/closed geometries, as well as highlighting any intermediate nonlinearities.

II.a. Method

The experiment was performed using a B-foot Boehm flute with the head joint replaced by a recorder mouthpiece, as shown in [fig. 1](#). This allowed for better control over the reproducibility of the blowing pressure. This “hybrid flute” was excited by air flow from a ResMed S8 air pump of variable fan speed. Two different single-key fingerings were analysed. The first was a semitone transition from what would normally be F#4 to F4 ($\sim 370 \text{ Hz} \leftrightarrow 349 \text{ Hz}$), however due to the recorder head the instrument was detuned (slightly sharp) so that $F\#4 \approx 381 \text{ Hz}$ and $F4 \approx 359 \text{ Hz}$. The fingerings used for this transient are shown diagrammatically in [fig. 2](#). This is a somewhat unconventional fingering for the $F\#4 \leftrightarrow F4$ transient, however it is still used in some cases, mainly for an F4 trill. This transient will be referred to below as the *trill fingering* transient.

Since there is already some difficulty involved in measuring the frequency during the transition, a semitone difference does not leave much room for error. The second fingering involved a major third in tone difference, from F#4 to D4 ($\sim 370 \text{ Hz} \leftrightarrow 294 \text{ Hz}$), once again detuned to $F\#4 \approx 378 \text{ Hz}$ and $D4 \approx 300 \text{ Hz}$. See [fig. 3](#) for fingering diagrams. Note that the fingering for this transient is fairly artificial and would not normally be used, except perhaps as part of a multi-key transition. However, this compromise was allowed in order to restrict the analysis to single-key transients (most traditional single-key fingerings only play a semitone). The transient will hereafter be referred to as the *cross fingering* transient.



Figure 1: *Left:* Photograph of recorder mouthpiece in place of flute head. The difference in diameters was padded with thread tape, and the joint was also plugged with a removable adhesive to prevent leakage. *Right:* Photograph of ResMed S8 air pump used to supply constant blowing pressure.



Figure 2: Diagrams of the fingerings used for the trill transient, created using the Virtual Flute tool (<http://flute.fingerings.info>) *Left:* Fingering used for F4. *Right:* Fingering used for F#4.

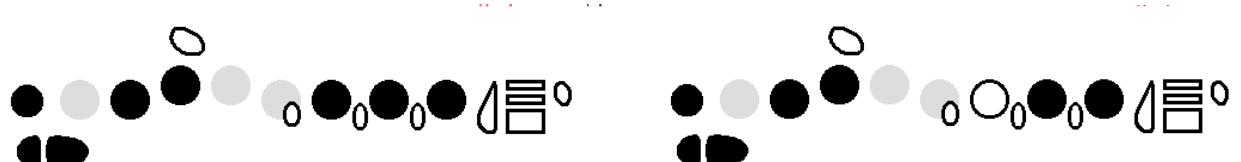


Figure 3: Diagrams of the fingerings used for the major third transient, created using the Virtual Flute tool (<http://flute.fingerings.info>) *Left:* Fingering used for D4. *Right:* Fingering used for F#4.

The key was initially open to the mechanical limit, and its position was incrementally adjusted using an acrylic “finger”. At first, a flat mechanical finger was used, however due to the curvature and angle of the flute key this made it unreliable to correlate the displacement of the finger with displacement of the key. A second round of measurements was taken after a convergent acrylic point was added to the finger. This is demonstrated in the photograph in [fig. 4](#). Datasets from both methods are used in the report, so for the sake of distinction the mechanical setups will be referred to as the *flat finger* and the *point finger* respectively. In this section ([II](#)) all the presented results are for the point finger. The finger was attached to a micrometer gauge with a Vernier scale. Audio was recorded at multiple locations using different microphones:

- Rhode NT3 microphone - labium signal
- Brüel & Kjær 4944-A pressure-field microphone - internal signal (bore)
- An omnidirectional tie-clip microphone to monitor the external signal (near key)

Since the zero-aperture key position is difficult to define, the key position was recorded in increments of 0.25 mm from the mechanically open limit.

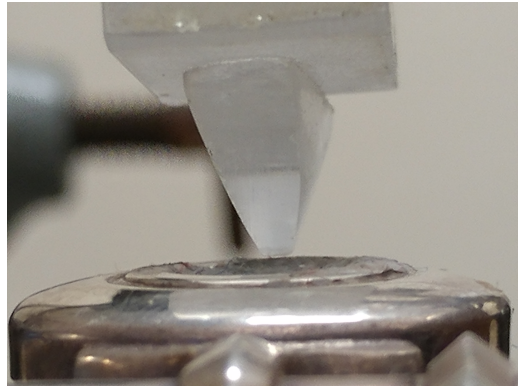


Figure 4: Photograph of the improved acrylic “finger”. The added point was aligned with the groove in the key, to restrict unwanted sliding.

II.b. Results

The results for fundamental playing frequency and sound level extracted from the audio are shown in [fig. 5](#) and [fig. 6](#). It is clear that these are following a nonlinear behaviour. Error bars show the standard deviation for three trials. For both fingerings, saturation of the frequency is observed at the effectively open/closed geometries. Note that the major third transient (larger Δf) requires a larger geometry change to saturate the acoustics at the new note. Furthermore, the power loss and frequency instability during the final stages of the transition are greater.

Plots of (a) f0 frequency and (b) sound level against closing increment

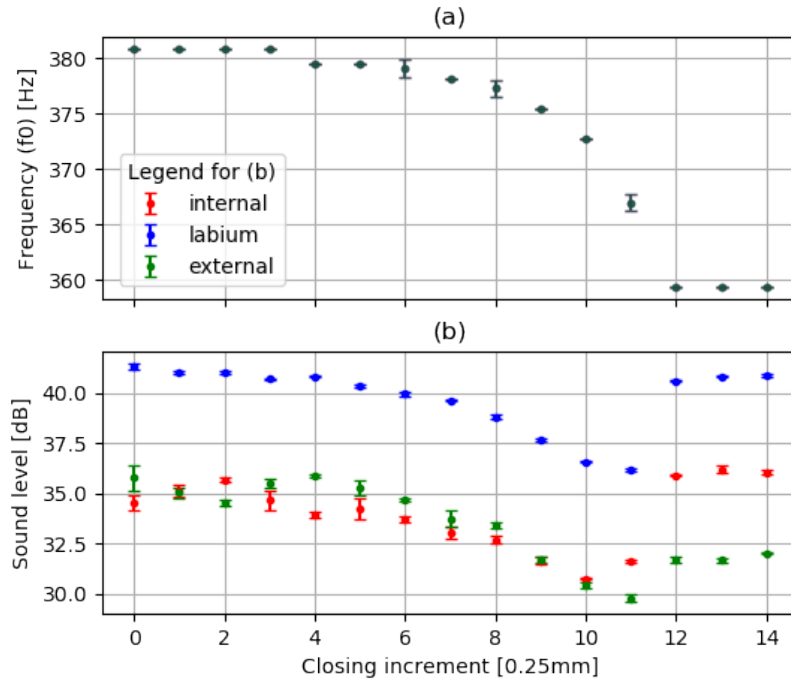


Figure 5: Trill fingering results for playing frequency and sound level at static transition geometries.

Plots of (a) f0 frequency and (b) sound level against closing increment

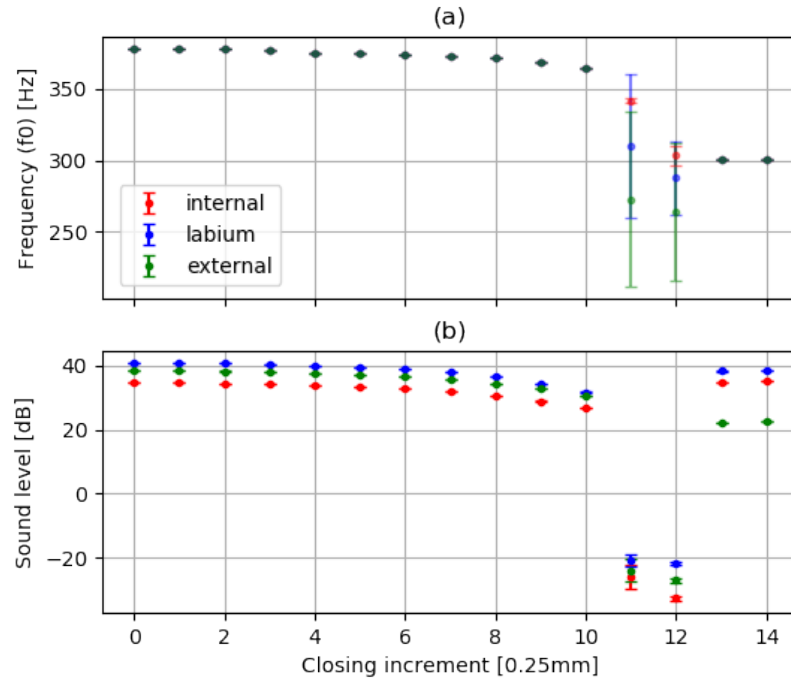


Figure 6: Cross fingering results for playing frequency and sound level at static transition geometries.

Both frequency and sound level of the audio were obtained using Discrete Fourier Transform (DFT) techniques. A flat top windowing function was used to reduce scalloping loss when obtaining the amplitudes of the playing frequency f_0 . However, any DFT method will always involve some level of approximation. For this project, the Python package *scipy.signal* was used to construct the windowing function, and the *numpy.fft* package was used for the fourier transform.

III Inertial properties of static geometries

In the previous experiment, it was established that the frequency of the transient note does not exhibit a binary change during the mechanical transition. In fact, the variation in f_0 was not even linear. To understand why this is the case, it is necessary to briefly introduce the acoustical concepts involved. The inertia of the air below the key controls the flow moving in and out of the tone hole. This is measured by the *acoustic inertance* \mathcal{L} , which is inversely proportional to the flow area. The inertance of an open tone hole affects the pressure profile in the bore, modifying the frequencies of the resonant modes [8]. It was worth investigating this effect for intermediate key positions, since this could yield a more direct method for relating mechanical and effective geometries.

III.a. Method

In order to better isolate the effects of inertance changes from closing a single key, only the foot joint of the flute was used. Photographs of the experimental setup are provided in [fig. 7](#). It was plugged at both ends, to prevent other acoustical end effects. A pair of tie-clip microphones were positioned at a tone hole about half way down, inside and outside the hole respectively. The other keys were taped shut to prevent flow leakage. An external loudspeaker provided a broadband sound which was used to measure the acoustical transfer function between external and internal receivers. An airborne transfer function such as this is defined simply as:

$$ATF \text{ [dB]} = \frac{P_{int}}{P_{ext}} \quad (1)$$

where P_{ext} and P_{int} are the sound pressure spectra at the external and internal locations respectively. In this experiment, to help remove any baseline, these were first divided by reference spectra obtained with both microphones outside the resonant volume. This removed the need for direct calibration of the microphones. As before, the key was closed in 0.25 mm increments.

III.b. Results

Due to limited amounts of data for the point finger setup, the flat finger results for this experiment, using the original acrylic block, will also be presented. [Fig. 8](#) shows a plot of transfer function (TF) spectra obtained for various key openings. For decreasing aperture values, the resonance peak moves to lower frequencies and loses power. Finally, the resonance peak is lost completely as the transition is made to the acoustically closed state.

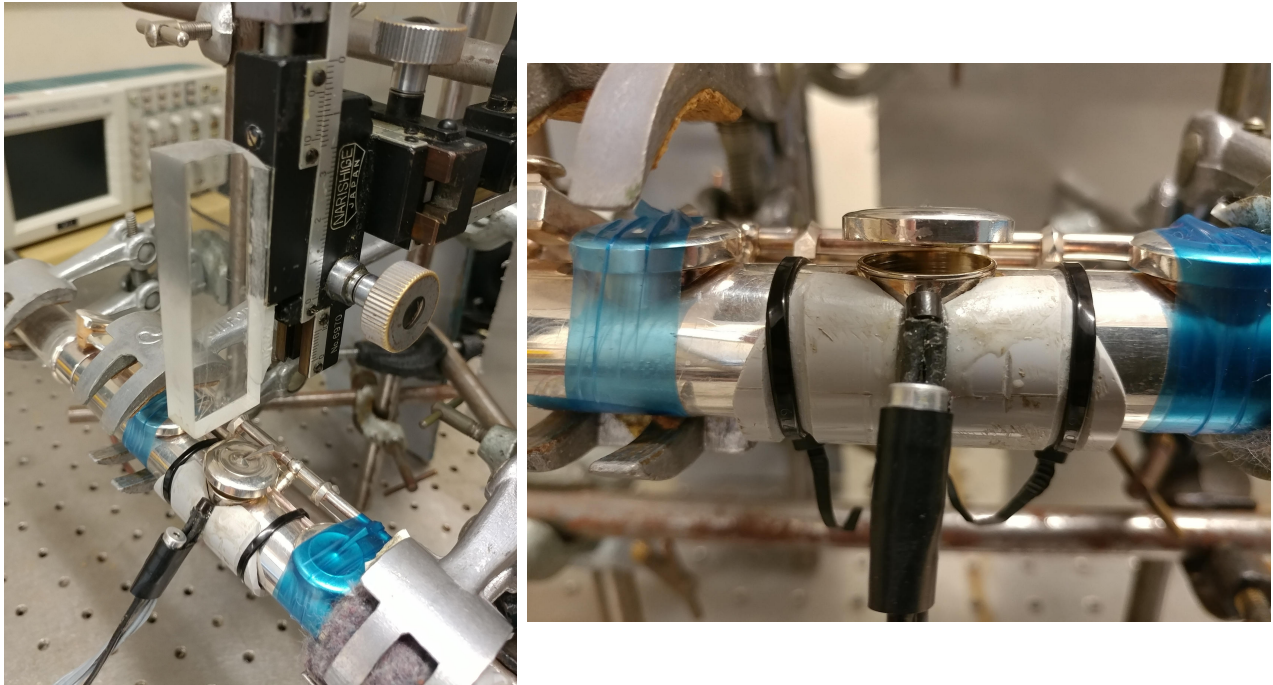


Figure 7: Photographs of Boehm B-flute foot as set up for transfer function measurements. **Left:** Micrometer setup. Note that in this picture the “flat finger” is still used. **Right:** IR sensor setup (see section IV.b.).

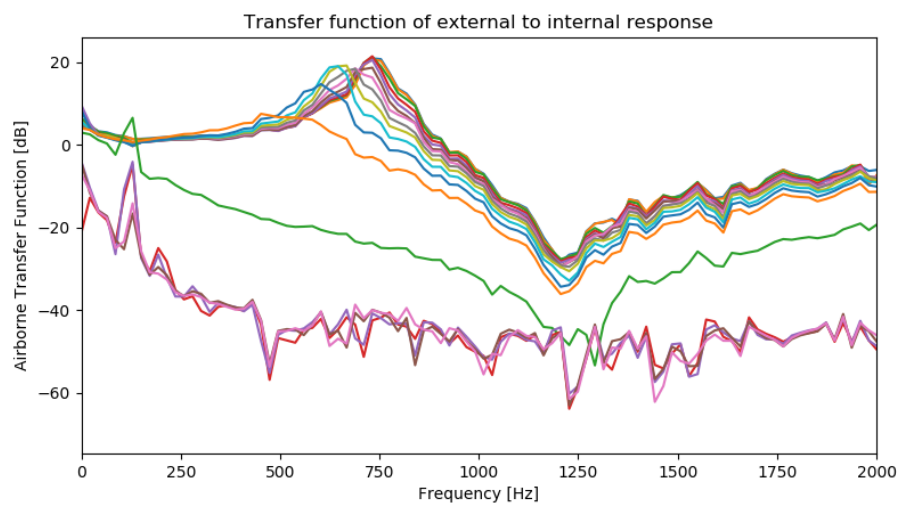


Figure 8: Example transfer function plot for the flat finger setup showing the resonance peak of the internal response decreasing from approx. 750 Hz. Note that here the data is plotted prior to lowpass filtering.

Forward-Backward (zero phase shift) lowpass filtering was used in processing the TF data. This allowed for better estimates of the resonance peak. The peak is directly, if non-trivially, related to the inertance of the air at the tone hole. This provides a second method for exploring the acoustical effects of transitional geometries. Experimentally, this is an easier method, since there is no need for the flute to be played and only two signals are recorded. However, the theory involved is more difficult (see p. 10).

A plot of the peak frequency as a function of closing increment is shown in [fig. 9](#). The effectively open/closed states are once again determined from the frequency saturation levels. For both acquisitions, the frequency transition occurs over 1.75 mm of aperture change, however the transition is shifted by 0.25 mm for the second acquisition. This could simply be caused by reproducibility problems with the flat finger setup, as explained in section [II.a.](#), and demonstrates the motivation for introducing a second setup.

The results from the point finger setup are shown in [fig. 10](#), and the transition occurs over 2 mm of aperture change consistently. The frequency offset compared to the first setup was possibly caused by the use of a different plug which could have decreased the resonant volume. The new plug was better sealed and could be held by a third clamp, decreasing the strain of the bore due to stress applied by the acrylic finger.

For the flat finger acquisitions, a simple white noise spectrum was used to produce this noise source, however for the point finger setup a summation of sine waves was implemented.

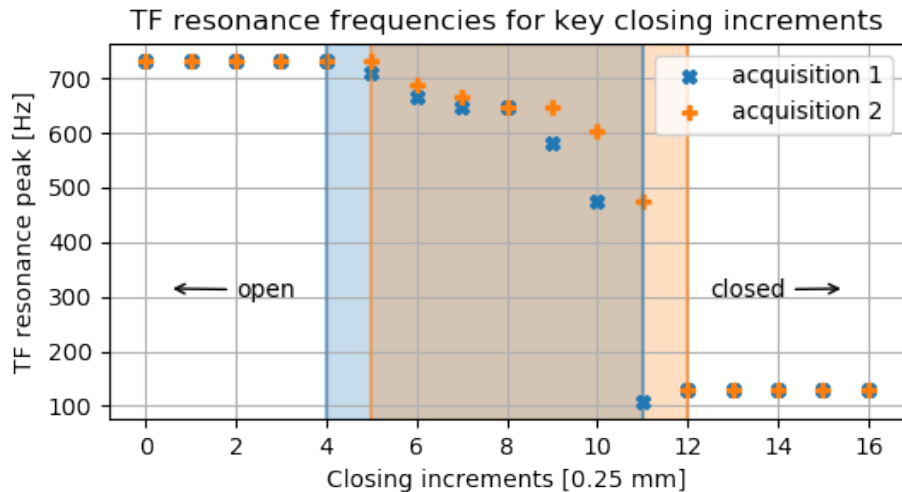


Figure 9: Plot of resonance frequency for static key displacement (from 0 at mechanically open) for preliminary acquisitions (flat finger). The shaded regions highlight the geometry change required for frequency transition. The shift in these regions is caused by sensitivity to geometric reproducibility.

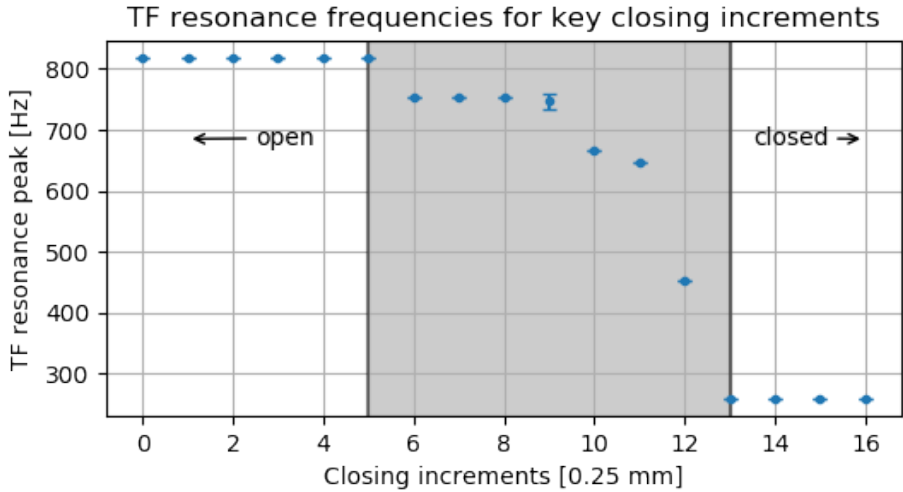


Figure 10: Plot of resonance frequency for static key displacement (from 0 at mechanically open) for point finger acquisitions. The vertical lines mark frequency saturation levels. The standard deviations from three trials are plotted as error bars, but are barely visible on this scale. This indicates improved reproducibility.

We see that out of the 16 aperture increments, only about half are acoustically relevant. However this ratio does not facilitate practical analysis. Firstly, due to the compression of the pads and pliability of the instrument, the mechanical limits of the key are not well resolved on the order of 1 mm. Secondly, the results from part II suggest a dependence on the spectral range of the transition.

Nevertheless, the above plots do give some indication of the acoustical response at transitional geometries. Departure from saturation at the higher resonance is followed by a region where changes in geometry have almost no effect. Then most of the frequency variation occurs over a small range near the closing saturation. Note the similarity in shape to the playing frequency response in [fig. 5](#).

With the goal of formulating an acoustical model that would explain these findings, we started from an established theory. The response of a Helmholtz resonator is well studied, and bears some relevance here. Helmholtz resonance occurs when fluid oscillations are produced in a small “neck” attached to a larger, rigid container. The static fluid mass within the neck is excited by an air jet or external sound source. Its inward motion compresses the volume in the vessel, causing an increase in pressure. Elasticity of the resonator volume pushes the neck mass out again. It travels further than the equilibrium position due to the excitation energy, which in turn creates a pressure decrease, and an inward restoring force. The harmonic oscillations produced in this way are equivalent to the behaviour of a mass on a spring, as shown in [fig. 11](#) below.

Depending on the geometry, a particular resonance frequency is established. This Helmholtz frequency f_H is related to the geometrical dimensions A (cross-section of the aperture) and V (resonator volume) by the formula:

$$f_H = \frac{c}{2\pi} \sqrt{\frac{A}{V \cdot L}} \quad (2)$$

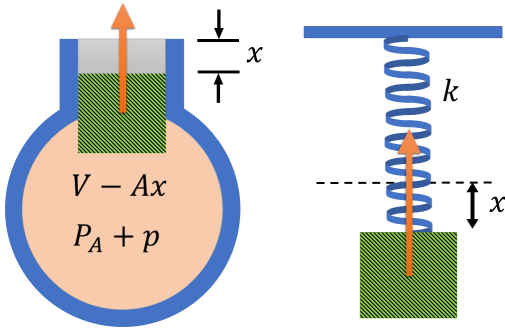


Figure 11: Diagram of Helmholtz resonator, with the “neck mass” (green) displaced into the original volume V , causing a pressure gradient (P_A is the outside pressure) [9]. The resulting restoring force (orange) is analogous to the force for a spring with a mass displaced from the point of rest.

where c is the speed of sound (approx. 343 m s^{-1} in air). The effective length L is defined as the geometrical length of the neck after modification to include acoustical end effects. This is a crucial parameter in the case of this investigation. While the aperture A (between the key and the tone hole chimney) and volume V (bore volume of the flute section) can be measured experimentally, the acoustical effects of the key itself dominate over those of the tone hole chimney (i.e. neck), especially for small apertures. Therefore the effective length is in this case more of a characteristic end effect of the key. Specifically, the acoustic inertance \mathcal{L} of the air below the key can be related to L by the formula [10]:

$$\mathcal{L} = \frac{\rho L}{A} \quad (3)$$

where ρ is the density of air (approx. 1.2 kg m^{-3}).

The relevant dimensions of the flute foot are shown in fig. 12, giving a volume of $V \approx 1.74 \times 10^{-4} \text{ m}^3$. The flow aperture A is the band between the lip of the tone hole chimney and the key. It can be calculated by multiplying the circumference of the chimney by the key aperture. Here the first complication arises, since the hinged construction means that the aperture is not uniform on all sides of the tone hole. For the particular flute used in this project, it was measured that the aperture was three times smaller on the hinged side. This ratio was approximated as being independent of the small variations in key angle. The corrected aperture was then taken as the average, i.e. two thirds of the measured value.

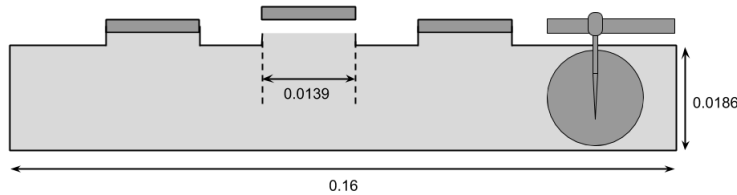


Figure 12: Diagram of Boehm B-flute foot with open key showing relevant dimensions in metres.

By algebraic manipulation of eqs. (2) and (3) we can calculate the experimental values for inertance and effective length using:

$$\mathcal{L} = \left(\frac{c}{2\pi f_H} \right)^2 \frac{\rho}{V} \quad (4)$$

$$L = \frac{A}{\rho} \mathcal{L} \quad (5)$$

These values are recorded in table 1 for the complete TF resonance dataset. As expected, the inertance of the air beneath the key increases for smaller apertures, and the relationship is nonlinear. The end effect produced by the key can equivalently be measured as the effective length of the resonator neck. The data demonstrates that this effect is dominant. The calculated value for effective length is over three times larger than the aperture height when approaching effective opening, and almost six times larger when approaching effective closure. This indicates the need for deeper investigation into end effects caused by the key in order to fully understand the nonlinear behaviour during a transient.

Increment	Resonance	$\pm \sigma$	Inertance	$\pm \sigma$	Effective length	$\pm \sigma$
0	835.49	23.59	149.63	36.40	10.11	0.65
1	835.49	23.59	149.63	36.40	9.29	0.56
2	835.49	23.59	149.63	36.40	8.47	0.48
3	835.49	23.59	149.63	36.40	7.65	0.42
4	835.49	23.59	149.63	36.40	6.83	0.36
(2.00 mm) 5	831.18	19.26	151.52	39.13	6.07	0.25
(1.75 mm) 6	775.20	30.45	173.03	38.53	6.08	0.27
(1.50 mm) 7	766.58	19.26	177.81	45.08	5.25	0.29
(1.25 mm) 8	762.28	11.79	180.31	48.29	4.32	0.44
(1.00 mm) 9	745.05	24.55	191.31	61.71	3.46	0.30
(0.75 mm) 10	667.53	45.68	244.00	94.96	3.01	0.51
(0.50 mm) 11	555.56	179.13	279.61	112.55	1.88	1.05
(0.25 mm) 12	374.68	106.15	402.90	0	1.47	1.34
(0.00 mm) 13	258.40	0	-	-	0	0
14	258.40	0	-	-	0	0
15	258.40	0	-	-	0	0
16	258.40	0	-	-	0	0
-	[Hz]		[Pa m ⁻³ s ⁻²]			[mm]

Table 1: Table of averaged results for TF resonance analysis. Due to limited data, the flat finger results were included. The frequency offset discussed on p. 8 is not relevant to the transient analysis, and was removed by normalising the closing saturation frequencies. Errors are the standard deviation from the total of 5 trials. The red font indicates results between effectively closed/open geometries. The aperture size relative to effective closure is given in brackets.

It is worth noting the limitations of the Helmholtz model. Sound waves, like any wave phenomenon, have an associated phase at any given instant. Since “sound” is essentially oscillations in pressure, the phase describes the instantaneous local pressure. [Equation \(2\)](#) requires an implicit assumption: that the phase is homogeneous inside the resonant volume. This assumption is reasonable if the wavelength of the resonance is very large compared to the size of the resonator. Taking 750 Hz as the resonance frequency, we have $\lambda = 0.46$ m. The largest resonator dimension is 0.16 m, which makes the assumption less than ideal in this case.

IV Characteristics of real-time transients

The previous sections have focused on the acoustics of static conditions, since these are easier to control experimentally. However, observations made for these snapshot geometries do not fully describe the dynamic response during a note transient. Analysis of real-time transients is necessary to verify the acoustical characteristics, and to study how these are affected by transient speed.

The trill and cross fingering transients described in [section II](#) were played manually at a variety of speeds. *Audacity* software was used to manage recordings, however this meant that the sound amplitude was automatically normalised. It was therefore necessary to calibrate the audacity scale to a corresponding pressure level in order to obtain more meaningful results.

Furthermore, the vernier scale could not be used to measure live changes in key displacement, however this had been anticipated. During the static measurements an infrared sensor was also attached below the key, alongside the microphone (see [fig. 7](#)). This allowed for calibration of the IR sensor signal to the displacement as measured by the vernier screw gauge. Using this conversion, the instantaneous change in displacement of the key can be monitored during live transients.

IV.a. Sound pressure calibration

For the pressure calibration, a number of recordings were taken at static geometries. The RMS value of the sound waveform was extracted and from this also the amplitude envelope of the wave. This was automated with the help of algorithms already developed in this lab. The pressure detected at the B & K microphone was also recorded. Using linear regression the conversion from the 32-bit scale used in Audacity to an absolute pressure value was obtained. Due to issues with reproducibility and adjustments made to the signal amplification, the calibration was performed for each of the transients. The linear fits are shown in [fig. 13](#).

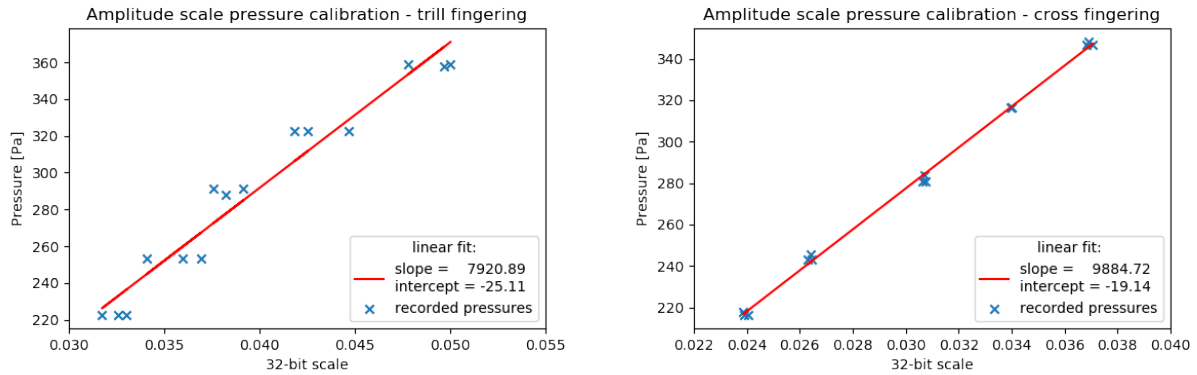


Figure 13: Pressure calibration for the trill fingering transient (left) and the cross fingering transient (right). The slope and intercept values define the linear equation for converting normalised amplitude to pressure.

IV.b. Key displacement calibration

The displacement calibrations were performed using a Kodensi SG-2BC infrared sensor, consisting of an infrared LED and a phototransistor. To minimise undesired sensitivity to environment lighting, the LED output was modulated with a 10 kHz sine wave. Once again the calibration was performed for each fingering. The results are shown in fig. 14. Note that difficulties were encountered in obtaining consistent infrared sensor results. The sensor was affected by small variations in position or angle and was difficult to stabilise, and for live transients the reading could vary based on shadows or overhang of the player's finger. Thus the standard deviation errors presented in the graphs should be taken as only minimum indications.

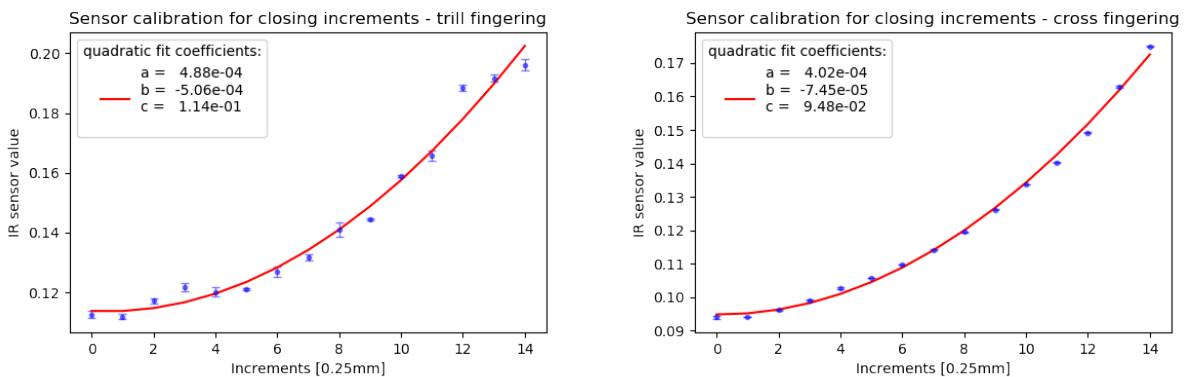


Figure 14: Displacement calibration using infrared signal, for the trill fingering (left) and cross fingering (right) transients. Error bars are standard deviations from three trials.

Calibration was further complicated by the apparent nonlinearity of the IR sensor response. Modelling the response involves many variables such as the intrinsic response of the device, the radiation angle relative to the key lip, and the reflectivity of the key lip. Instead, a quadratic regression fit was used as an approximation. The coefficients are listed in fig. 14 for the

quadratic equation:

$$y = ax^2 + bx + c \quad (6)$$

where y is the sensor value and x is the closing increment, which can be converted to a relative displacement. In order to find the instantaneous speed of the key, the following relation is used:

$$\frac{dx}{dt} = \frac{dx}{dy} \frac{dy}{dt} \quad (7)$$

where dy/dt is measured experimentally for the manual transients and dx/dy is defined for positive x and $y \geq c$ as:

$$\frac{dx}{dy} = \frac{1}{2ax + b} \quad (8)$$

with x the inverse function of eq. (6):

$$x = \frac{\sqrt{b^2 - 4a(c - y)} - b}{2a} \quad (9)$$

Substitution of eq. (9) into eq. (8) yields the simplification:

$$\frac{dx}{dy} = \frac{1}{\sqrt{b^2 - 4a(c - y)}} \quad (10)$$

IV.c. Results

The focus of the preliminary live-transient analysis presented here was restricted to the same parameters as the static analysis. In particular, the effects of transient speed on frequency gradient and pressure gradient were tested.

The key displacement was obtained by extracting the RMS amplitude of the IR sensor signal and calibrating according to the quadratic fit in fig. 14. This was converted to a speed value using numerical differentiation (`numpy.gradient`). Comparison of the entire speed evolution is not easily applied to many transients. However, significant information can still be obtained by comparing the maximum speed which the key reached during each transition.

Using the speed maxima as pointers, snippets of audio could be extracted and analysed. Since preliminary tests had shown that the frequency tended to change rapidly during a transient, it was unlikely that the Fourier Transform method would give the desired frequency resolution. Instead, the frequency of each cycle within the audio snippet was calculated from the time between zero crossings. The maximum frequency gradient was extracted for comparison. Scatter plots of maximum frequency gradient against maximum key speed are shown for both closing and opening transients in figs. 15 and 17.

The pressure gradient was obtained in a similar way, after the audio amplitude had been calibrated according to the linear regression in fig. 13. Once again, the maxima were used for comparison. Scatter plots of maximum pressure gradient against maximum key speed are shown in figs. 16 and 18.

Colours represent different recordings. Note that the key speeds are significantly slower for spring-controlled opening.

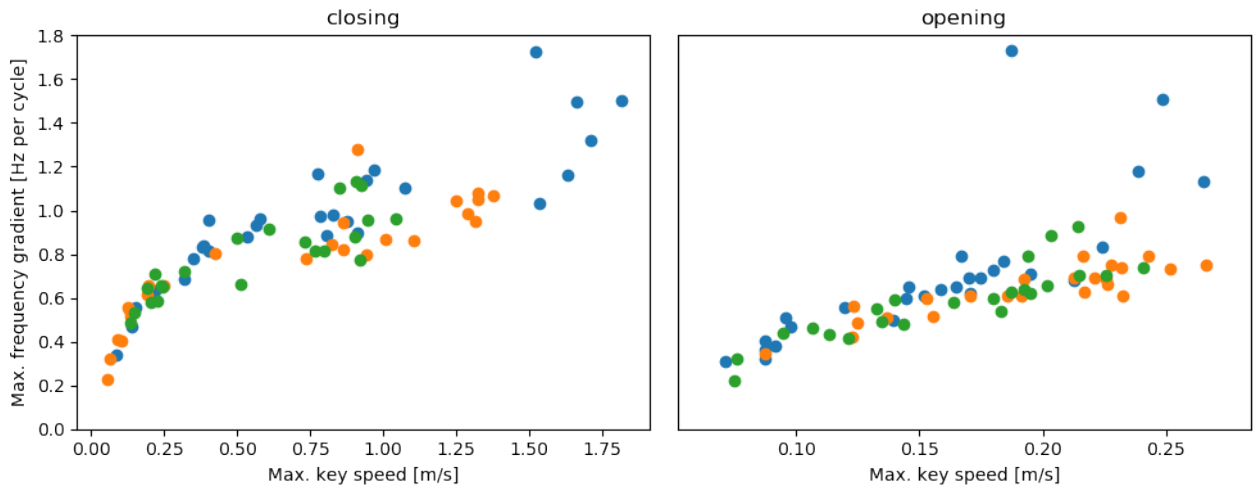


Figure 15: Maximum frequency gradient vs maximum key speed for trill fingering transients. At low speeds (below 0.25 ms^{-1}) the relationship for both opening and closing transients is roughly linear. For fast closing transients, however, the maximum frequency gradient does not scale. This reinforces the expectation that the speed of the acoustic transition has an upper limit unrelated to the mechanics.

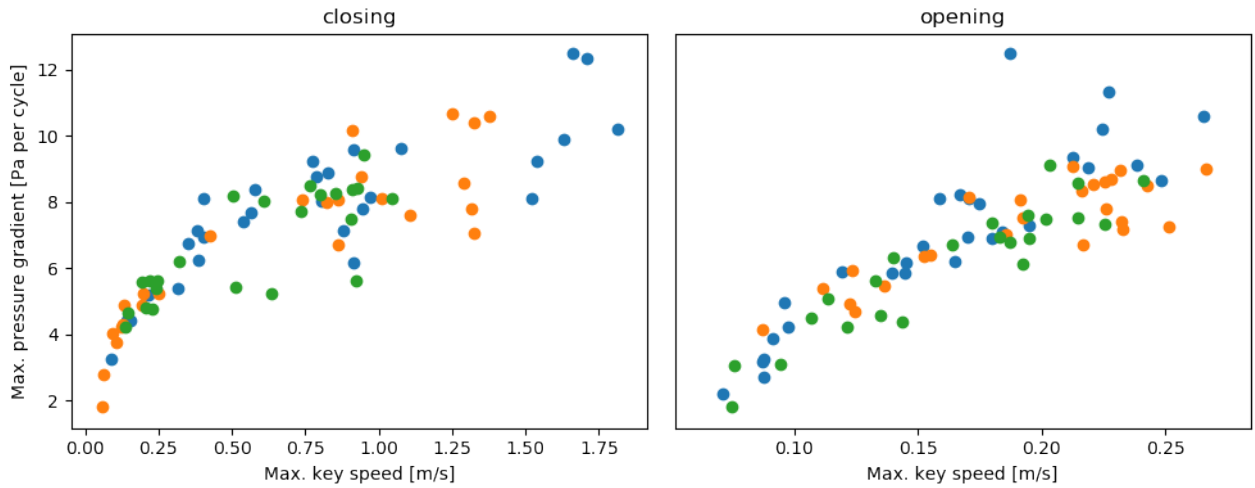


Figure 16: Maximum pressure gradient vs maximum key speed for trill fingering transients. The correlation is similar to frequency vs speed. However, the pressure results show a greater nonlinearity. It is possible that this is the result of insensitive calibration. Nonetheless, it is interesting that the sound level behaves the same as the frequency for different transient speeds.

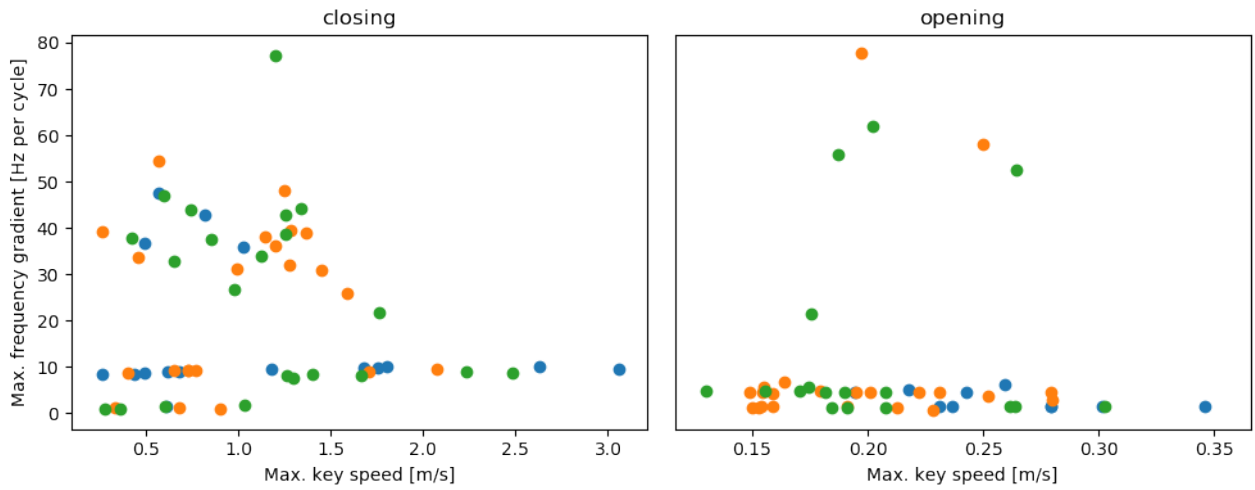


Figure 17: Maximum frequency gradient vs maximum key speed for cross fingering transients. The results are not as clear as for the trill fingering. A few transients reach large frequency gradients (perhaps due to octave jumps), however most do not change by more than ca. 10 Hz per cycle. This reinforces the trill fingering result that the maximum frequency gradient is upper bounded. If this is the case, then the main result from section II seems plausible: transients with larger frequency range will saturate slower.

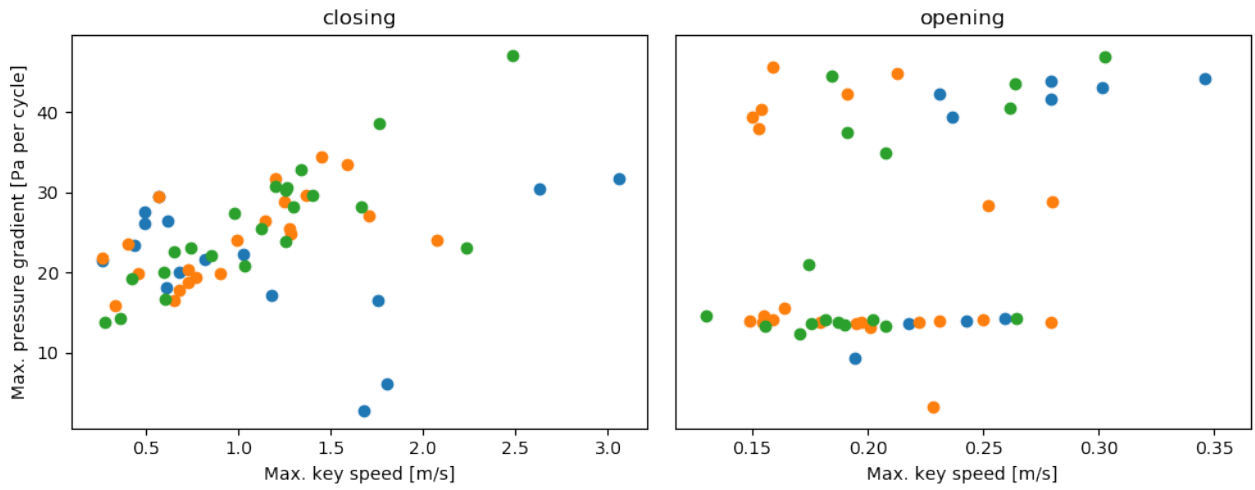


Figure 18: Maximum pressure gradient vs maximum key speed for cross fingering transients. Unlike for the trill fingering, the pressure gradient does not seem to follow the same behaviour as the frequency gradient. Some similarities can still be found, such as the pile-up of pressure gradient maxima at around 15 Pa per cycle for opening transients. However, the results for the cross fingering are largely inconclusive.

V Conclusion

Studying flute transients is a deceptively complicated and sensitive task, owing to both the speed of the transient and the ingenuity of the mechanical construction. Two methods were explored as possible means of studying transient acoustics using static regime responses. By regulating the blowing pressure and using a mechanical finger to hold the key at intermediate openings, it is possible to isolate some of the transient characteristics. However, this method requires a reproducible playing setup and one would be inclined to use the complete instrument. The second method allows for some experimental flexibility, as it is more directly concerned with the effect of the key; the “instrument” serves only as a Helmholtz resonator. The portion of the flute used for this project does not represent such a resonator very well, and care should be taken to match the Helmholtz approximation more closely in future research. This report demonstrates the viability of both methods, and highlights the importance of geometric reproducibility and the significance of end effects caused by the key.

In general, it was found that the evolution of the acoustic response during a transient is nonlinear. Both frequency and sound level are most affected by a near-closed key. The observations presented seem to suggest that for transients with a larger spectral range, the geometry change required for saturation at the new note is also larger. This naturally means that large Δf transients will have a longer duration when played in real-time. For the real-time recordings, key speeds could reach over 2 m s^{-1} for player-controlled closing, but tended to stay below 0.25 m s^{-1} for spring-controlled opening. Maintaining a distinction between opening and closing transients could prove useful in future analysis.

References

- [1] *Recent progress in the acoustics of wind instruments*
N. H. Fletcher, Acoust. Sci. & Tech, 22(3) (2001), p.169
- [2] *The effect of blowing pressure, lip force and tonguing on transients: A study using a clarinet-playing machine*
W. Li, et al., J. Acoust. Soc. Am. 140(2) (2016), p.1089
- [3] *The mechanism producing initial transients on the clarinet*
A. Almeida, et al., J. Acoust. Soc. Am. 142(6) (2017), p.3376
- [4] *The role of initial attack and performer expertise on instrument identification*
J. Cassidy, A. Schlegel, Int. J. Music Educ. 34(2) (2016), p. 186
- [5] *Feature dependence in the automatic identification of musical woodwind instruments*
J. C. Brown et al., J. Acoust. Soc. Am. 109 (2001), p.1064
- [6] *Sound-source recognition: A theory and computational model*
K. D. Martin, PhD Thesis, Massachusetts Institute of Technology, Cambridge, MA, (1999)
- [7] *The kinetics and acoustics of fingering and note transitions on the flute*
A. Almeida, et al., J. Acoust. Soc. Am. 126(3) (2009), p.1521

- [8] *The Acoustics of Woodwind Musical Instruments*
J. Wolfe, Acoustics Today [Advance Online Publication], available at:
<http://acousticstoday.org/acoustics-woodwind-musical-instruments/>
- [9] Helmholtz diagram and mathematical derivations available at:
<https://newt.phys.unsw.edu.au/jw/Helmholtz.html>
- [10] Derivation of the inertance equation can be found at:
<http://www.animations.physics.unsw.edu.au/jw/compliance-inertance-impedance.htm>